Marching of the microlithography horses: Electron, ion, and photon: Past, present, and future

Burn J. Lin
Taiwan Semiconductor Manufacturing Company, Inc.
8 Li-Hsin Rd. 6, Hsinchu Science Park
Hsinchu, Taiwan 30077 R.O.C.

ABSTRACT

Microlithography patterning employs one of three media; electron, ion, and photon. They are in a way like horses, racing towards the mainstream. Some horses such as electrons run fast but repel each other. Ion beams behave like electron beams but are less developed. The photon beam is the undisputed workhorse, taking microlithography from the 5-μm minimum feature size to 32-nm half pitch. This paper examines the history of microlithography in pattern generation, proximity printing, and projection printing, then identifies the strong and weak points of each technology. In addition to ion-beam and e-beam lithography, the coverage of optical lithography spans the wavelength from 436 to 13.5 nm. Our learning from history helps us prevent mistakes in the future. In almost all cases, making or using the mask presents one of the limiting problems, no matter the type of beams or the replication method. Only the maskless method relieves us from mask-related problems. A way to overcome the low throughput handicap of maskless systems is to use multiple e-beam direct writing, whose imaging lens can be economically and compactly fabricated using MEMS techniques.

In a way, the history of microlithography parallels that of aviation. Proximity printing is like the Wright-Brothers' plane; 1X projection printing, single-engine propeller plane with unitized body; reduction step-and-repeat projection printing, multi-engine commercial airliner; scanners, jet airliners. Optical lithography has improved in many ways than just increasing NA and reducing wavelength just as the commercial airliners improving in many other areas than just the speed. The SST increased the speed of airliners by more than a factor of two just as optical resolution doubled with double exposures. EUV lithography with the wavelength reduced by an order of magnitude is similar to the space shuttle increasing its speed to more than 10 times that of the SST. Multiple-beam direct write systems are like helicopters. They do not need airports(masks) but we need a lot of beams to carry the same payload.

Keywords: Microlithography, e-beam lithography, ion-beam lithography, optical lithography, x-ray lithography, EUV lithography, microlithography history, microlithography outlook

1. Introduction

Microlithography, a specific technology used to pattern IC circuits as early as 1958, is coming to its 50th anniversary. Initially, it was as straightforward as ancient-day lithographers replicating patterns carved in stone masks. However, as circuit dimensions continued to shrink, more care had to be taken for microlithography. Very early on, people recognized that there was a limit to photon-based patterning techniques, higher energy particles or shorter wavelengths such as electrons and ions were proposed as the patterning carrier. "Optical techniques for fabricating devices are generally limited to > 5 μm linewidths in practical production by the diffraction effects", according to Herriot[1] in 1975. He must have in mind proximity printing at a large mask-to-wafer gap using near-uv wavelengths between 350 and 450 nm. In the same issue, deep-uv lithography using 250-nm wavelength was inaugurated[2] demonstrating 0.5-μm features for magnetic-bubble circuits. X-ray proximity at wavelength below 1 nm was also reported[3] in the same issue, along with e-beam writing on wafer[4,5,6], e-beam writing on mask[7], and e-beam projection printing[8]. These papers set the stage for things to come decades later.

In 1987, IC fabrication was predominantly done with optical steppers resolving 0.75-μm half pitch. Lin[9] wrote, "With successful reduction of the actinic wavelength and development of low k_1 technology, resolution as low as 0.18 μm is not impossible." Even though very aggressive at that time, it was still too pessimistic. He did not anticipate the advent of chemical-mechanical polishing (CMP) that planarized the topography on the wafer, reducing the minimum depth of

Optical Microlithography XX, edited by Donis G. Flagello, Proc. of SPIE Vol. 6520, 652002, (2007)
0277-786X/07/$18 · doi: 10.1117/12.720628

focus (DOF) requirement from 650 nm to less than 200 nm. Lin's prediction extended to 130 nm half pitch[10] by allowing optical proximity correction (OPC) to drop k_1 to 0.44 at 193-nm wavelength and 0.65 NA. He again was pessimistic in the required DOF and the maximum NA attainable at a 26-mm diameter field. The prediction recently extended to 19 nm half pitch[11]. Now it is time for the particle means or x-ray photons to realize their potential.

2. Microlithography and horses

The different branches of microlithography are like horses. Optical lithography is obviously the workhorse. It has been bearing the manufacturing burden since the >5-μm era to reach[12] eventually 19 nm, an advance of 16 generations from 11 to 0.1λ. Innovation, economy, infrastructure and momentum have been keeping the optical horse commissioned. E-beam lithography in its early days was like racehorses. Electrons move fast. Patterns can be written with individual beam spots at great speed. However, these racehorses tend to repel each other. It is against their nature to pattern a large number of pixels with many electrons together. Therefore, even though the electron horses[7] overpower the photon horses in writing mask patterns with single beam, multi-photon-beam (MPB) mask writing has proven to have higher throughput than single-electron-beam mask writing[13]. If the space charge effect of electrons is contained to allow multi-electron-beam (MEB) operation, e-beam horses can be as productive as photon horses. Ion beams, in many ways, are similar to electron beams, except that they are less nimble and less affected by space charge. The development of ion-beam imaging systems often lack behind that of e-beam systems. Therefore, the ion beam can also be considered as a racehorse but rather younger and more immature, thus, baby racehorse.

Each beam can perform in four ways for patterning just as horses have four legs. Each beam can perform direct writing on mask or wafer. It can proximity print without using an imaging lens. It can also projection print through an imaging lens. In this case, the printing can either be 1X or NX reduction. For the wavelength or energy that does not allow for the operation of all four legs, the technology may not be that useful. Take 1-nm x-ray. The lack of imaging lens removes it from projection printing thus the leverage of NX reduction. For 13.5-nm extreme ultraviolet (EUV), having to operate always in the reflective mode, eliminates the possibility of proximity printing. It makes early-phase resist development expensive, the mask-protecting pellicle impossible, and necessitate the use of reflective mask which puts severe demand on substrate flatness and smoothness. Reflective optics also has the handicap of low NA.

2.1.1. Advantage of reduction lithography

The reduction advantage is significant. Table 1 shows critical dimension (CD) tolerance for the 4X, 1X, and direct write systems. The RMS sum of the CD tolerance comprises variation due to contribution from the mask resist image, mask

Table 1 Comparison of CD tolerance in NX, 1X, and direct write systems. (a) MEF=1 (b) MEF=4.

MEF	CD Tolerance	4X	1X	Direct Write
1.00	$Mask_{Resist}$	3.33%	13.33%	
	$Mask_{Etch}$	1.67%	6.67%	
	$Wafer_{Resist}$	7.00%	7.00%	8.00%
	$Wafer_{Etch}$	3.50%	3.50%	3.50%
	Other Contributions	2.50%	2.50%	2.50%
	RMS Sum	9.02%	17.02%	9.08%

(a)

MEF	CD Tolerance	4X	1X	Direct Write
4.00	$Mask_{Resist}$	13.33%	53.32%	
	$Mask_{Etch}$	6.67%	26.68%	
	$Wafer_{Resist}$	7.00%	7.00%	8.00%
	$Wafer_{Etch}$	3.50%	3.50%	3.50%
	Other Contributions	2.50%	2.50%	2.50%
	RMS Sum	17.02%	60.19%	9.08%

(b)

pattern etching, wafer resist image, wafer pattern etching, and other miscellaneous contributions such as film non-uniformity and metrology errors. Changing the mask contribution according to the reduction ratio while keeping the

other contributions identical, the NX system is better than the 1X system by a factor of 1.89 in case (a). Note that at the same RMS sum, direct write systems allow a larger tolerance in the wafer resist image, because there is no mask contribution. In present day manufacturing, the mask error factor (MEF) can be as high as 4 making the mask contribution more significant. Case (b) demonstrates this situation. The RMS sum of either projection system becomes worse but with the 4X to 1X improvement raised to 3.54. In this case, the direct write system has a clear advantage even after allowing more tolerance at the wafer resist image.

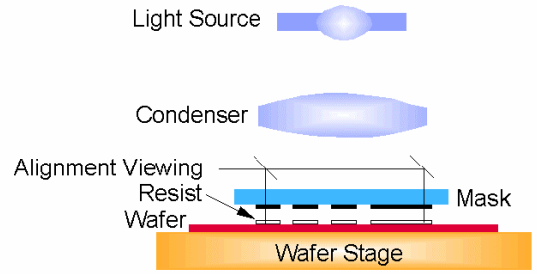

Figure 1 Schematic of a proximity printing system.

3. The proximity printing leg of the horses

Proximity printing is depicted in Figure 1. There are the light source, illuminator, mask, and resist on the wafer. No imaging lens between the mask and the wafer is needed. This not only makes it easy to manufacture IC, the common components to projection printing systems, such as the light source, the mask, and the resist, can be tested for development before the projection lens of the right wavelength and NA becomes available. It is not surprising that the photon and the electron horses take advantage of it. Deep uv lithography[2] started with proximity printing. Same is <1-nm x-ray[14,3]. E-beam also took advantage of proximity printing[15,16].

Freedom from the imaging lens also means less cost, no lens distortion or other aberrations, field size not limited by the imaging lens, and DOF identical to the working distance which has to be between 10 and 20 μm to prevent mask or wafer damages. However the disadvantage of damage outweighs the advantage of large DOF. Having the mask and wafer at two imaging planes for the alignment system presents another difficulty. Because of unity magnification, it is difficult to fine tune magnification for alignment. One often resorts to thermal or mechanical means than optical means. By far 1X mask is the most severe concern. Not only the reduction leverage is lost, 1X mask writing requires a high-resolution mask writer. 1X features also become sub-wavelength for earlier technology nodes than those in reduction systems. Last but not least, the mask pellicle has become an indispensable part of modern day high-yield IC fabrication. With short working distance, mask pellicle is impossible. The short working distance also makes the mask vulnerable to accidental contacts to the resist surface, particulates or wafer topography, not to mention resist outgassing during exposure.

From the point of view of diffraction, it is puzzling that proximity has carried optical lithography from 5 to 2 μm. Figure 2 shows the electric and magnetic field distribution[17] in x, as a function of mask-to-wafer distance z. Figure 2(a) depicts

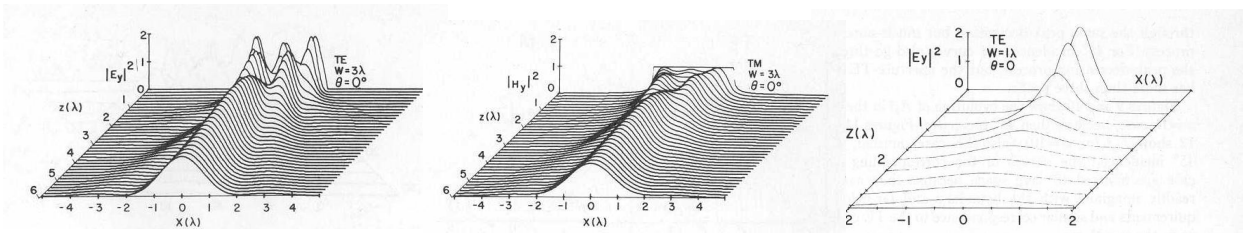

Figure 2 Diffraction from medium slits. (a) Electric field distribution from a 3λ wide slit illuminated with TE illumination. (b) Magnetic field distribution of same size slit with TM illumination. (c) TE electric field distribution from a 1λ slit.

the situation of transverse electric field (TE) illumination where the electric field vector is parallel to the edge of the slit that points in the direction of the y axis. The slit is 3-wavelength wide. At the contact plane, the electric field forms a high-contrast image with the same number of peaks as the number of wavelength of the slit width. As z increases, the image smoothens out, then become high contrast again but the number of peaks are reduced to two. Eventually the image focuses to a single-peak image, then gradually spreads out as it goes through the Fresnel, then Fraunhofer

diffraction regions. Figure 2(b) depicts the magnetic field from the same slit but with transverse magnetic (TM) illumination; Figure 2(c), TE illumination as in (a) but the slit width is 1 λ. When the illumination is monochromatic and spatially coherent, the diffracted image is rich in structure as shown in Figure 3, which is the resist image of the diffracted light from a close proximity of 6.6λ slits[18]. In the early days of proximity printing, the illuminating light was broadband, spatially incoherent, and unpolarized, the mask-to-wafer distance was not uniform nor well controlled, the lucky combination makes CD variation as a function of exposure and mask-to-wafer gap the only observable. Later, with x-ray proximity printing using synchrotron as light source, people initially tend to boast the purity in wavelength and spatial coherence of the light source until they realized that those are handicap and had to scramble the light for better images[19,20,21]. Of course, the membrane mask in x-ray proximity printing makes it more difficult than uv or deep-uv proximity printing. However, it is impressive that x-ray proximity printing could be managed to print 100-nm features[22]. The ability of x ray to penetrate very thick resist is being taken advantage for MEMS applications[23].

Figure 3 Four-peaked resist image taken from 6.6λ slits at close proximity to the slits.

4. Marching of the ion-beam lithography horse

Ions are thousand times heavier than electrons but carry the same amount of charge per particle. As a result, it takes more energy to move ions. Ions also carry much more energy to remove or change the property of the materials they bombard. Larger mass also enable they to be more efficient with resist exposure, less affected by space charge as well as stray electric and magnetic fields. The technologies that take advantage of the specific properties of ions tend to be developed more fervently. For example, ion-beam mask repair[24] has been broadly used until the introduction of e-beam mask repair recently[25]. In a way the popular ion-beam applications can be viewed as ion-beam proximity printing. For example, ion implantation is usually masked with a patterned resist image in contact to the substrate. Reactive ion etching also uses either a resist or an inorganic pattern to mask the pattern transfer, ditto with ion milling. Recently, there is a proposal to take advantage of the large DOF of ion-beam proximity image for curved surfaces[26]. Direct writing ion-beam machines were available as early as 1979. Seliger et al[27] reported micromachining, doping, and resist exposure with focused 55kV gallium ion beam. However, ion-beam direct writing never took off for large-scale wafer manufacturing, except for repair of mask or devices. Focused ion beams are also used for dissecting devices for failure analysis[28]. As for the projection legs with ion-beam lithography, 4X reduction projection has been pursed for a long time[29],[30],[31]. In principle, 1x ion-beam projection is possible but there has never been an opportunity to warrant this application.

5. Marching of the photon-beam lithography horse

Photon-beam lithography is no doubt the workhorse of the semiconductor industry, pulling it along since feature size was in the 5-μm regime. It is still strong, manufacturing circuits with 45-nm features. It will stay for at least two other technology nodes. The evolution of optical microlithography is in many ways similar to that of the aviation industry. The technology will be presented with this perspective in mind.

5.1. Optical proximity printers as the Wright-Brothers' planes

The proximity printing system resembles the airplane of the Wright Brothers' era. As discussed in Section 3, proximity printing systems are easy to build just as the Wright Brother's planes. The working distance is short for proximity printing, ditto for these planes. They had a cruising speed of 34 mph and some of the early flight range was as short as 120 ft. The mask is prone to contaminations and damages for lack of protection just as the pilot of these planes being vulnerable to environmental hazard, because of lack of enclosure.

5.2. 1X full-field projection printers and single-engine airplanes with unitized body

Offner[32,33] et al invented the 1X full-field projection printing system by taking advantage of the good imaging ring-field zone of two concentric mirrors as shown in Figure 4. Here the slit field is a section of the full-circle ring field. It is turned 90^0 with the prism block so that the mask and the wafer can be scanned in the same direction. In addition to just facilitating the turning of the slit fields, the prism block has an extra mirror to convert the projected image to a mirror

image so that the projection-printing mask is compatible with proximity printing masks. This is a big step forward from proximity printing because there is now ample working distance. The mask is well isolated from particles on the wafer. Similarly, the single-engine airplanes with unitized body, exemplified by the North American P-51 Mustang, can travel as far as 950 miles. It has a top speed of 437 mph. There is a canopy keeping the pilot away from potential contamination and destruction from the environment. The full-field projection printer is a precision instrument that requires special skills to build, similar to the unitized-body planes.

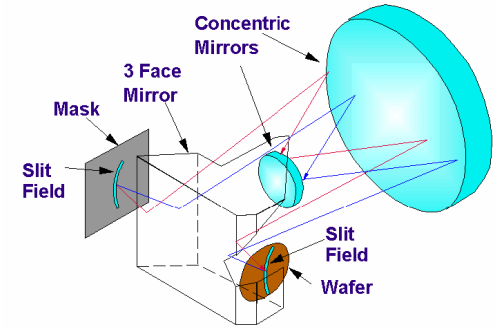

Figure 4 1X scanning full-wafer projection printing system invented by Offner and co-workers.

5.3. Step-and-repeat projection printers and airliners with multiple propeller engines

The numerical aperture(NA) of the ring-field field system is limited to 0.18. In the 1980s when no resolution enhancement technique was available, it was necessary to use $k_1 \equiv (W/\lambda)NA \geq 0.8$ for satisfactory imaging. This imaging lens with the band of wavelengths centering to the Hg I-line at 365 nm can only resolve 1.6-μm half pitch while reducing the wavelength to the deep-uv regime centering at 254 nm, can resolve no better than 1.1 μm. On the other hand, using the Hg g-line at 436 and NA=0.28 can resolve 1.25 μm half pitch. It was comparably easy to increase the NA using dioptric solid-field lens systems at the expense of field size. Full-wafer exposure can no longer be sustained. In fact, with the continuous growth in wafer size beyond 125 mm, the ring-field system cannot support full-wafer exposure even at NA=0.18. Hence, the step-and-repeat system comes into existence. A field much smaller than the wafer is stepped repeatedly on the wafer until the exposure completely populates the wafer. Early steppers were built by Canon, Inc. The FPA120 was introduced in 1973. Its NA is 0.2 at λ = 405 and 436 nm, field size = 20x20 mm^2 after 2X reduction. In 1975, a canon 4X reduction system was introduced, supporting a 10x10 mm^2 field at NA=0.31. The stepper was popularized by GCA corp., combining a solid-field lens with an interferometer-controlled stage for positioning the steps and for alignment. It owes its success to the interferometer stage and computer control. A schematic drawing of this type of exposure tool is shown in Figure 5.

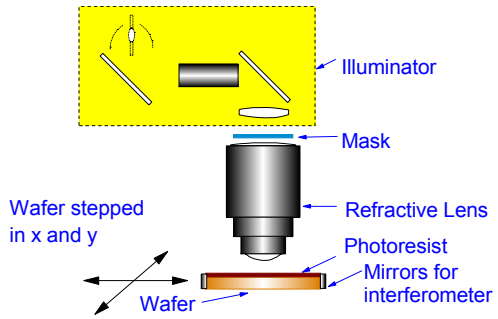

Figure 5 A schematic step-and-repeat projection-printing system.

These multiple-field exposure systems remind us of the multi-engine propeller airliners, exemplified by the Lockheed Constellation which has four propeller engines. The Constellation weights 12 times more than the Mustang. Its range is at least three times longer. However, its speed is slightly less. Similarly, the stepper has a lower throughput but it carries more pixels to the wafer.

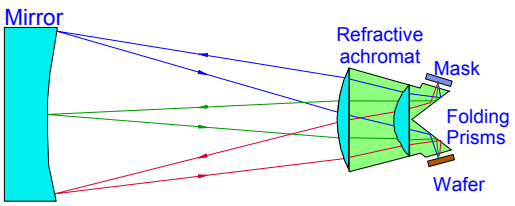

Figure 6 Wynn-Dyson lens and a field splitting prism.

Note that there were many different reduction ratios, 10X, 5X, 4X, 2X, and 1X. The field size of the 10X system is simply too small to sustain. A 1X system from Ultratech[34], using a catadioptric Wynn-Dyson lens with a field-splitting prism depicted in Figure 6, was very economical because of large field size, low aberration, and small number of optical elements, thus, low construction cost. However, the 1X mask prevented it from resolution below 0.5 μm. One reason was lack of reduction leverage in CD control and in overlay accuracy. The former was discussed in Section 2 and the latter in Reference 9. Moreover, the features on the mask quickly approaches wavelength dimension. For example, 0.5 μm is only slightly larger than the g-line 436-nm wavelength. The DOF budget has to allow for full mask placement and

flatness errors instead of just $1/n^2$ in nX systems. Last but not least, 1X masks are difficult to make. Hence, similar to proximity printing systems, mask is also a limiting factor for 1X projection systems.

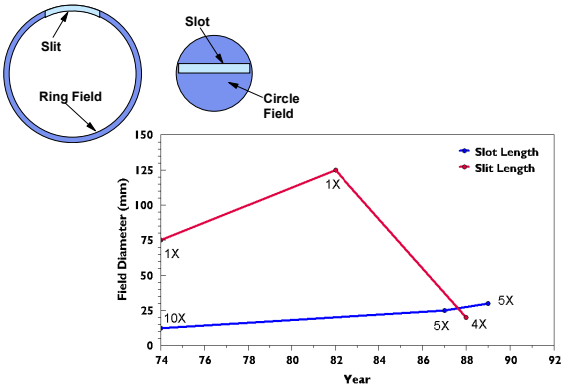

Figure 7 Slot and slit in circular and ring fields.

5.4. Step-and-scan projection printers and jet airliners

As semiconductor ICs continues to shrink and the number of pixels per field continues to move up, there is a need to increase the exposure field size. However, the growth of reduction circular field systems was slow, except for reduction from 10X to 5X, as shown in Figure 7. Naturally, one would resort to scanning just as in the full-wafer case. Hence, the step-and-scan system from Perkin Elmer[35] as depicted in Figure 8. The slot scans the entire mask and the wafer simultaneously. Because of reduction, the scanning speeds of the mask and the wafer differ by the reduction ratio. After the entire field is scanned, the wafer steps to a new field position. Scanning in a reverse direction is then performed so save the time for retracting the slot. With step-and-scan, the field size in the scan direction is only limited by mechanical constrains instead of optical ones.

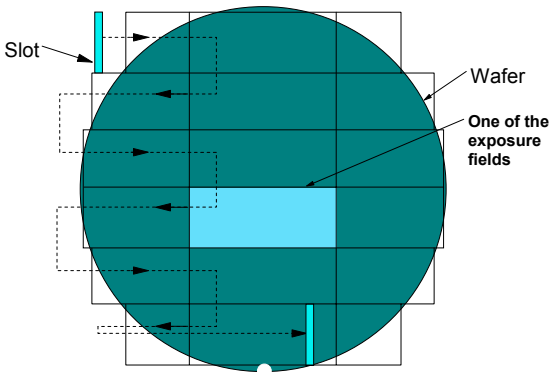

Figure 8 Step-and-scan principle.

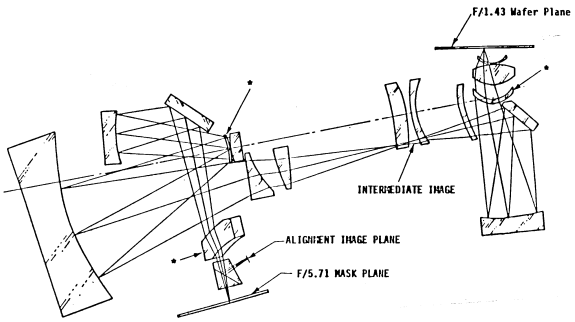

Figure 9 γ-prime 4X 0.35NA catadioptric deep-uv ring-field lens

In 1974, the field size of 1X ring field systems was much larger that of circular-field systems as shown in Figure 7. The rate of increase for the ring field system was also faster. However, as 1X systems gave way to nX systems, the slot length of ring-field systems dropped below the slot length of 5X circular-field systems. It made much more sense to use a wide straight slot that the circular slit. This move opened up the possibility of extremely high NA imaging lenses. The NA of the 1st step-and-scan system was 0.35. It used multiple optical axes and a catadioptric ring-field lens called γ-prime is shown in Figure 9. With six mirrors and six optical axes, it was very difficult to align. The chance of getting higher in NA was extremely low. Hence, a beam splitter was used to produce a circular-field 4X 0.35 NA catadioptric system as shown in Figure 10. The beam splitter was polarized, thus, there was no energy loss in the output beam. Otherwise, 75% of the incident power would be lost. The NA of this type of lens progressively increased

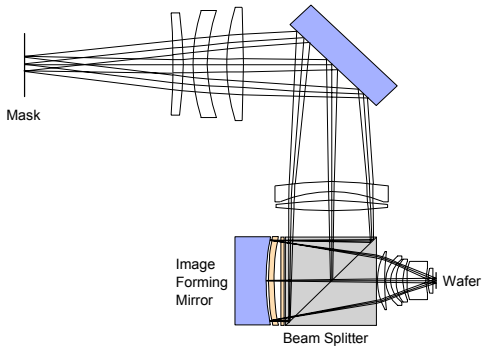

Figure 10 Catadioptric 4X reduction lens system using a beam splitter.

to 0.75 NA in a recent 157-nm scanner[36].

Scanner systems similar in configuration of a step-and-repeat system using dioptric imaging lens followed, soon after the introduction of the scanners using the circular-field catadioptric system. These lenses lend themselves to even higher NA. It reached 0.93 in air[37]. With water immersion, the highest NA planned[38] is 1.35. Figure 11 shows the design progression of several high-NA dioptric lens systems[39] from 0.7 NA to 1.1 NA. The latest is, of course, a water-immersion lens. When the NA is raised above 1.2, catadioptric systems have to be used to reduce the number of optical elements. History does go in circles.

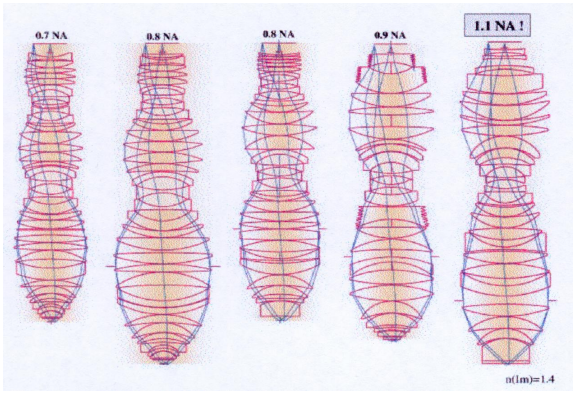

Figure 11 Dioptric 4X reduction lens systems.

Moving from step-and-repeat systems to step-and-scan systems is similar to airplane propulsion moving from the propeller age to the jet age, exemplified by the introduction of the Boeing 707. Its top speed at 607 mph almost reached the speed of sound, Mach 0.92. It is 39% faster than a very fast propeller airplane, the Mustang. The take-off weight is 75% larger than the Constellation and the range is 29%~114% longer depending on the fuel loading strategy.

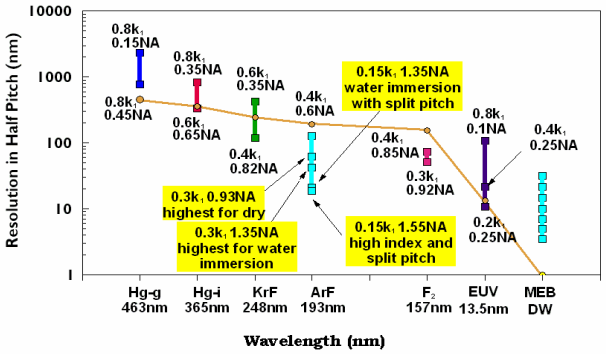

Figure 12 Progression of steppers and scanners.

5.4.1. More than just λ and NA

The progression of optical lithography based on the basic stepper and scanner configuration is plotted in Figure 12, the line across all wavelengths shows the actinic wavelength. The dimension of the optical images started at several times above wavelength and were reduced to sub wavelength by wavelength reduction and aggressive resolution enhancement indicated by reduction of the resolution scaling factor k_1. Further improvements of resolution include immersion lithography[40] and double patterning[41].

The progression of optical lithography in this era can be related to the progression of jet-propelled aircrafts from the Boeing 707 to the Boeing 747 and to the Concord Super Sonic Transport (SST). In the former transition, there was no gain in aircraft speed. It is actually 7% lower. However from 1960 to 1981, many other progresses other than speed have been made; namely fuel economy, takeoff weight, range, reduction of pollution and noise, passenger safety, comfort and entertainment. The Boeing 747 carries four times the takeoff weight and has 50% longer range than the Boeing 707. For lithography, many times the NA and wavelength improvements were too slow, progress was made from phase-shifting mask, off-axis illumination, optical proximity correction, reduction of vibration, immersion of the lens-to-resist medium, polarized illumination, and many other forms of illumination and pupil optimization.

In the transition from subsonic to supersonic transport, the cruising speed was raised by 140% while the takeoff weight is only 40% and range less than 50% of those of the Boeing 747. Getting to a not-so-far destination in half of the time at a much higher cost is really not what the users need. This situation is similar to improving resolution with double patterning. The cost of lithography nearly doubles. It may not warrant the gain in IC performance except in special cases.

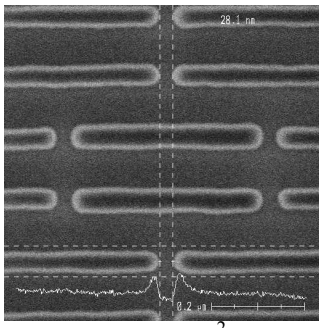
Figure 13 0.151 μm^2 SRAM imaged with an immersion scanner.

5.4.2. Limitation of nX masks

The nX reduction mask, allowing soft pellicles to protect the mask, is ideal. There is reduction leverage. Features on mask become sub wavelength four nodes later. The

use of pellicles prevents particles from falling on the mask to become systematic defect sources. However, even with these leverages, the nX reduction mask is also approaching its limit. A 32-nm feature is only 66.7% of the 193-nm wavelength even after multiplying the 4X magnification. There are usually sub resolution assist features or OPC produced jigs and jugs that are about 1/4 the minimum feature size, thus, 0.167λ. The 193-nm wavelength is sufficiently energetic to accelerate radiation-induced contamination on the mask, causing frequent cleaning and shortening the mask life. Increasing mask error factor (MEF) tightens the dimensional specs on the mask, making the mask writing, inspection, repair, and metrology equipment extremely expensive, thus, pushing up the mask cost. Cycle time is also prolonged because of the stringent specs as well as the complicated OPC operation. In short, the difficulty of mask making in no less than 1X masks in the early days.

5.5. Status of lithography at TSMC

TSMC had the opportunities to acquire three generations of ArF water immersion tool, ASML 1250i, 1400i, and 1700i. We have built electrically functioning product circuits at the 90-, 65-, and 45-nm nodes. The 1st work was a timely demonstration in 2004 with immersion imaging on the polysilicon layer[42]; the 2nd, in 4 critical front-end layers; the most recent node, in hundreds of wafer per day on 12-18 front-end and back-end layers. Figure 13 shows the after-etch image of a 0.151-μm^2 SRAM cell. Immersion lithography is run at single-digit number of defects per wafer, with overlay and yield comparable to those of dry systems in the 90- and 65-nm nodes. Researchers in many disciplines contribute to the success, amongst them: Theological analysis in the early days of immersion lithography in DOF[43], polarized illumination[44], image deterioration by bubbles in immersion fluid[45], and processing parameters for multiple technology nodes[46]; materials work to reduce defects such as switchable BARC[47], watermark reduction[48], and immersion hood cleaning[49]; process analysis such as algorithm[50] to pinpoint the location of particle leakage on the immersion hood, using super-positioned defect distribution chart, and speedy defect classification[51]. Figure 14 shows a super-positioned defect distribution chart with predicted particle leakage in red and actual particles in black.

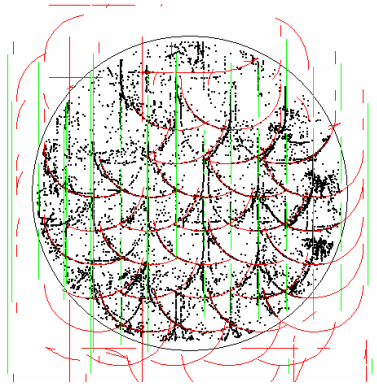

Figure 14 Display of defect trajectory followed with an algorithm to identify location of particle leakage on the immersion hood.

5.6. EUV lithography and the space shuttle

With 193-nm water-immersion lithography seemingly to reach its ultimate limit at 32-nm half pitch, at most by another 15% with 1.55 NA facilitated by high-index fluid and glass, a popular attempt is to reduce the water-immersion wavelength ten folds to 13.5 nm i.e. to EUV. At this new wavelength, resolution of 32-nm half pitch at NA=0.25 corresponds to k_1=0.59, similar to resolving 123-nm half pitch using 193 nm light at 0.93 NA. Currently the same imaging lens is used to manufacture features with 90-nm half pitch corresponding to a much lower k_1 of 0.434. Therefore, using a NA=0.25 EUV system to resolve 32-nm half pitch is relatively easy. Almost no low-k_1-related optical proximity correction is required. This advancement in lithography is similar to the advancement of the space shuttle from the supersonic transport. The take-off weight is more than ten times than that of the SST, ditto for the cruising speed.

EUV lithography (EUVL) has been explored[52,53] as early as 1989, aiming at taking over optical lithography in the 100-nm regime. Eighteen years latter, it has the opportunity to succeed optical lithography at the 32-nm half pitch. However due to many reasons, EUVL has not reached the manufacturing floor. They are listed as follows. This author has published a more detailed paper[54] earlier.

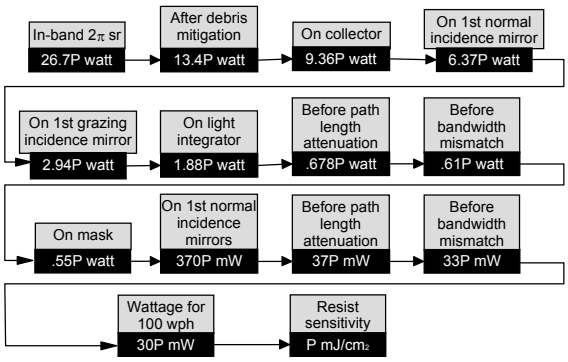

Figure 15 Power level at each EUVL component.

5.6.1. Tradeoff of source power, resist sensitivity, and linewidth roughness

EUVL has more power loss than longer wavelength projection printing systems, because it depends on reflection imaging. At a comparably high 0.25 NA for reflective systems, 6 mirrors are required. With condenser optics and the reflective mask, at least 9 reflecting surfaces are required. The reflectivity of each surface is built up from a multi-layer stack of Mo and Si up to 40~50 layer pairs for a theoretically maximum reflectivity of ~70%. So the power loss at each reflecting surface is about 30%. Together with loss due to radiation bandwidth, debris mitigation of the light source, grazing incidence mirrors, light integrator, and other causes, the power loss from the source to the resist is about 3-orders of magnitude as shown in Figure 15. Hence, due to the lack of high source power and the need of heat management, it is desirable to use very high resist sensitivity, preferably between 1 and 5 mJ/cm^2. However, high resist sensitivity leads to large line width roughness[55,56] (LWR) as seen in Figure 16. Resist sensitivity above 30 mJ/cm^2 is required for LWR < 5 nm. The required in-band EUV power at the source is correspondingly > 800 watt according to Figure 15. There is similar experience with resist sensitivity for 193-nm lithography. It is typically between 30 and 50 mJ/cm^2. Using realistic resist sensitivity drops the projected EUVL throughput by a factor of 3 to 5, with the same source power.

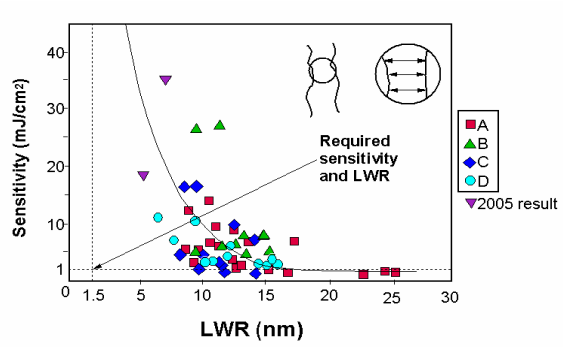

Figure 16 Trade-off between resist sensitivity and LWR for resists in 2004 and 2005. The experiments were performed by researchers at ASML. The asymptotic curve was drawn by this author.

5.6.2. Flatness of EUV masks

Because EUVL is a reflective system, the illumination beam to the mask has to make an angle to the optical axis perpendicular to the mask, typically 6 degrees. Any mask tilt and translation of the mask lead to image positioning errors as shown in Figure 17. Global mask tilt and translation can easily be compensated with the orientation and repositioning of the wafer. However, non-flatness and roughness on the mask, i.e. micro-orientation and micro-translation errors, inevitably induce lateral and longitudinal image positioning errors. The former is a source of overlay error.

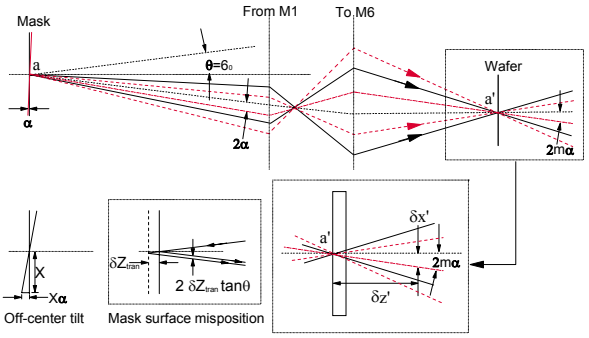

Figure 17 Lateral and longitudinal position errors due to mask rotation and translation.

Using 1/3 of the minimum feature as the overlay tolerance and 1/3 of this tolerance allocated for image positioning errors due to mask non-flatness, the mask needs to be flat[54] within 46 nm when α=0 and the minimum feature is 22 nm for 32-nm half pitch. With α>0, the tolerance is even more severe. Current best ArF mask flatness is 500 nm. Meeting the much more stringent flatness requirement adds more cost to the already very expensive blank.

5.6.3. Random phase shifting

Because of the extremely short wavelength and reflective mask, it is difficult to control pattern topography on the EUV mask for phase-shifting applications. Figure 18 shows that the step height A, either from an absorber or a trench, need only be 3.35 nm to produce 180^0 phase shift. If A is 0.11 nm, it already reaches the 6^0 tolerance for phase-shifting masks. When the localized topography on the EUV mask falls between 0.11 and 3.35 nm randomly due to process variations, random phase shifting takes place. The effect of random phase shifting is reduction of the common process window for the features on the entire mask as shown in Reference 54. Therefore, there is

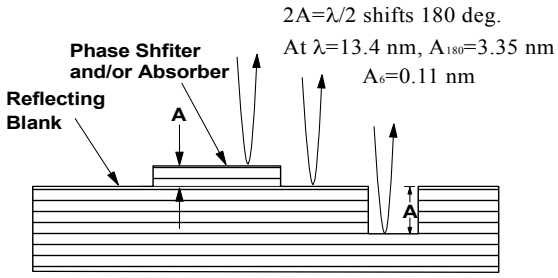

Figure 18 Random phase shifting in EUVL.

no benefit in using phase-shifting mask, if not creating more problems than binary intensity mask.

5.6.4. Cost of EUVL masks

It is a common perception that EUVL mask blanks are more expensive, because of the multi-layer substrate, stringent flatness requirement, and the need to keep it defect free. However, EUVL advocates propose that because of extremely simple OPC, the OPC data processing cost is saved and that because the patterns are much more straight forward, they are easier to write, thus, less expensive. This may be true at k_1=0.59 for 32-nm half pitch imaging but definitely false for k_1=0.41 and 0.33 for 22- and 15-nm half pitches. Even at k_1=0.59, higher stray light level, 3-D mask consideration, and absorber shadowing due to 6^0 illumination incident angle, the EUV image contrast is lower than that of 193-nm lithography, a higher level of OPC is expected. Other words, there is no reason that EUVL masks is cheaper than 193-nm masks. Perhaps the only saving is in not using a pellicle. Actually, manufacturing without a pellicle is extremely alarming as discussed below.

5.6.5. Absence of mask pellicles

Since very early on in optical projection printing, it has been a necessary practice to attach a pellicle to the mask to keep accidentally fallen particles out of focus to prevent printing defects. It is un-imaginable for a manufacturing process to use pellicle-less masks. Because of the extremely short wavelength, no material is transparent for EUV light, just as the reason for reflective optics in imaging and illumination. Therefore, opaque pellicles are used for EUVL masks to protect them during transportation, storage, loading, and unloading. During exposure, the EUVL mask has to be unprotected. This opens the possibility of debris from the light source and other types of particle in the vacuum system to attach to the mask. Electrostatic chucking for the mask increases such possibility.

5.6.6. Imaging difficulties for 22-nm and 15-nm half pitches

As given earlier, if the NA of EUVL system remains at 0.25 for 22-nm half pitch imaging and increased to 0.3 for 15-nm imaging, k_1=0.41 and 0.33, respectively. For 193-nm lithography to handle these low k_1 situations, many resolution enhancement techniques, such as phase-shifting masks, off-axis and polarized illuminations, scattering bars, and strong OPC, have to be used. For EUVL, phase-shifting mask is out of the picture. Off-axis and polarized illuminations are more difficult because of short wavelength and reflective optics. Coupling with higher level of stray light, these k_1 situations may not be manufacturable. It probably has to stay in the > 0.5 regime. The NA will have to be raised to 0.31 and 0.45 for 22-nm and 15-nm half pitches. Increasing NA inevitably necessitates more mirrors in the optical system, thus higher power sources to compensate for the reflection loss, not to mention the feasibility of designing and building such a system. The system in Figure 9 represents a very difficult system for reduction catadioptric ring-field optics at 250 nm wavelength. Extending a 13.5-nm reflective reduction imaging system to such NA regime with more than an order of magnitude tighter requirement on surface precision and roughness, capped with the small number of surfaces allowed, is similarly difficult if not more so.

6. Marching of the electron-beam lithography horse

In the many lithography systems discussed above, except for direct writing systems, the mask has always been a limiting issue. There is no exception for e-beam systems, either with proximity printing[15,16] or with projection printing[8,57]. The only way to avoid the mask problem is to use direct write systems. Any of the three means for imaging has direct writing capability. Direct writing with photon beams is obviously the first to be considered. The advantage of using photons is that the direct writing system can share the same resist with its replication counter part. However, with the same wavelength and NA limitations, the optical direct writing system cannot exceed the resolution limit of its replication counter part. Electron-beam direct-write systems, because of more energetic beam, equivalently much shorter wavelength, are not limited in resolution in the same sense of optical aerial images. An electron beam can also be positioned much faster than a photon beam. However, no matter how fast the beam can be positioned, the throughput of e-beam systems is much lower than that of optical systems, because the latter take advantage of massive parallelism. To overcome this inherent disadvantage, massive parallelism also has to be employed for e-beam systems; hence, the recent activities in developing systems up to 4M pixels in parallel. Ions have better resolution potential than electrons because of their shorter equivalent wavelength. However, as always, the baby horse lacks behind in maturity comparing with its older sibling.

We now show 3 MEB DW systems under development and use them as vehicles to demonstrate the challenges in MEB DW systems.

6.1. MEB DW system from MultiBeam Systems

One way to achieve multi-e-beam direct write is by clustering of existing e-beam micro-columns as exemplified by the EB-DW column block[58] shown in Figure 19. These columns including the sources are readily available commercially.

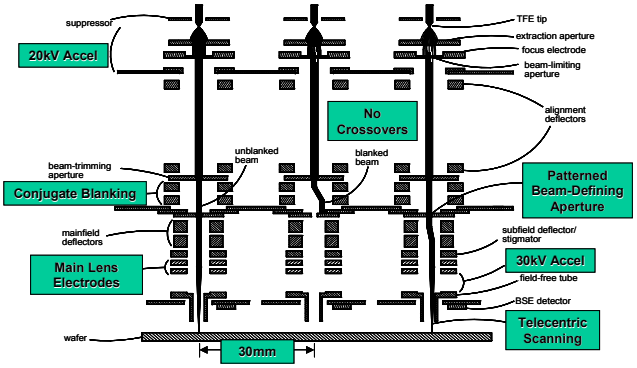

Figure 19 One-block EB-DW columns from MultiBeam Systems.

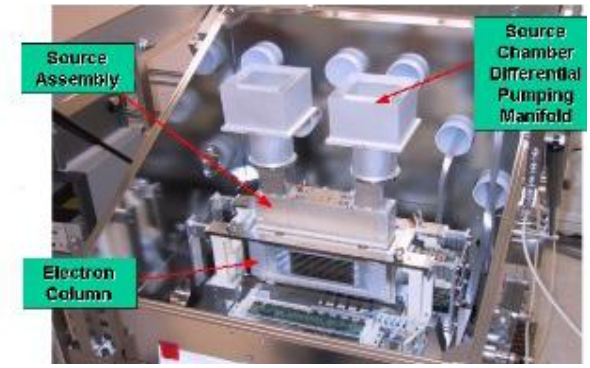

Figure 20 Micro-Columns of Multibeam Systems.

As many as 10x10 columns can be assembled for parallelism. In addition to the 2 orders of magnitude increase, the throughput is further increased with a proprietary projection scheme for rectangular patterns in single shots. It is a 50 kV system. There is no crossover in each column.

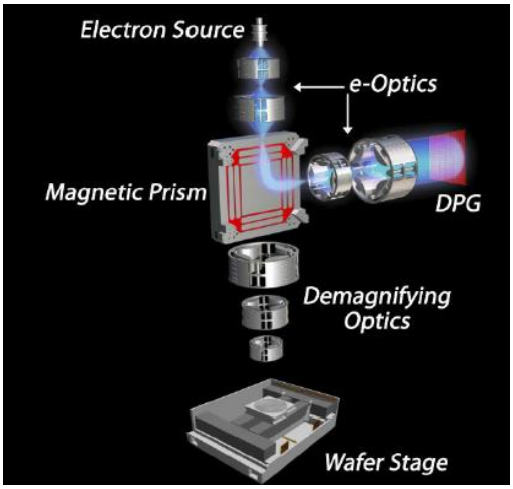

Figure 21 KLA-Tencor reflected e-beam lithography (REBL) system.

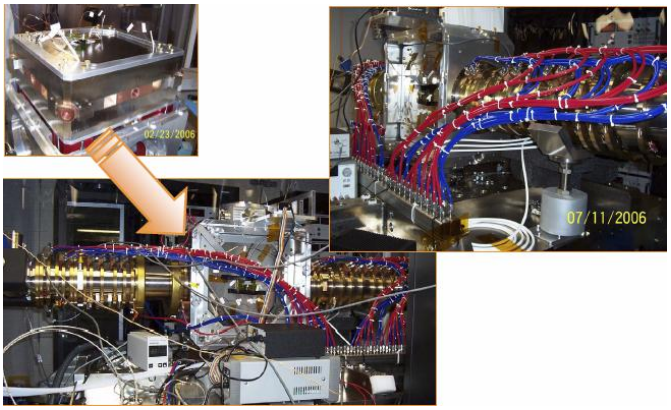

Figure 22 Transforming an inspection tool to REBL.

6.2. MEB DW system from KLA-Tencor

The KLA-Tencor system[59] uses up to 4M pixels in a programmable e-beam reflective mask consisting of CMOS circuits. As shown in Figure 21, the system starts with a conventional source collimated with standard e-beam optics. The beam is bent by 90^0 with a magnetic prism towards a reflective dynamic pattern generator (DPG). The reflected beam from the DPG is bent by another 90^0 towards the wafer by the same magnetic prism. This prism is equivalent to an optical polarized beam splitter. The DPG contains a CMOS circuit with its last metal layer facing the beam, the voltage on the 50-80 nm metal pads is used to switch the beam on and off. The required switching voltage is in the order of 1-2 volt because the incident beam is decelerated by the e-

beam optics between the prism and the DPG. The switched beam now accelerates towards the prism and is demagnified by the e-beam optics before reaching the wafer. The e-beam energy is 50 keV at the wafer. Crossovers are expected in the demagnification optics. All components except for the DPG, are taken from known systems for other purposes such as inspection. Figure 22 shows the conversion of an inspection tool into REBL.

6.3. MEB DW system from MAPPER

A 5-kV system[60] using MEMS and CMOS components is developed by MAPPER Lithography. As shown in Figure 23, The collimated e-beam from a single source is blocked into 13000 beamlets with an aperture plate. The beams reach the

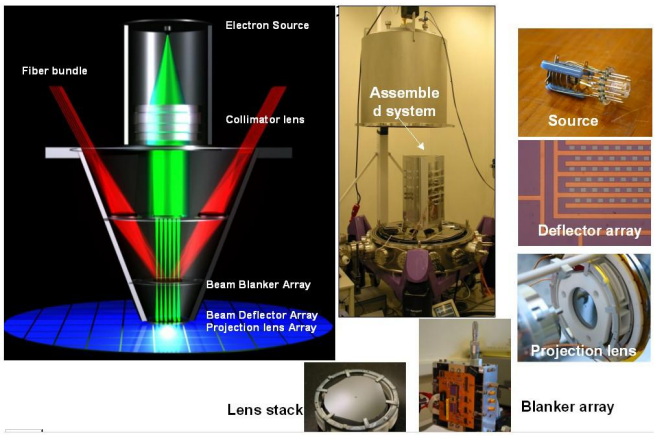

Figure 23 Configuration and components of the MAPPER MEB DW system.

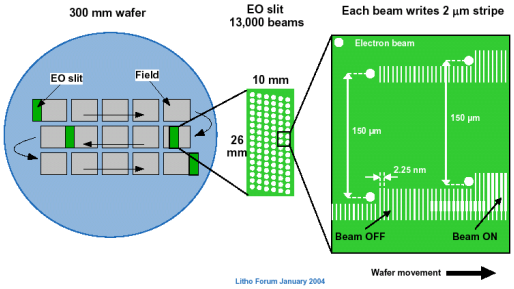

Figure 24 The MAPPER writing scheme.

blanker array consisting of CMOS circuits to amplify the electric signal induced by photons from the optical fiber. The amplified signal is used to blank the beams on and off. All beams are continuously deflected. The unblanked defected beams contribute to the written patterns. As shown in Figure 24, the beamslets are separated by 150 µm from each other to avoid space-charge interactions between them. There is no crossover throughout the entire electron optic. The deflection range is 2 µm for each beam. Continuous mechanical scanning takes place in the other direction. By properly staggering the beam apertures, patterns are stitched from the 2-µm coverage. The 26x10 mm^2 writing head is similar in

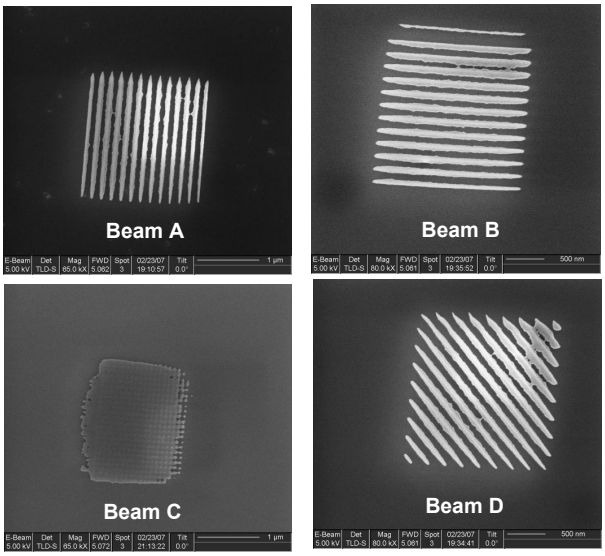

Figure 25 Recent pattern-writing results from optical fiber switching through the imaging assembly to the resist on wafer.

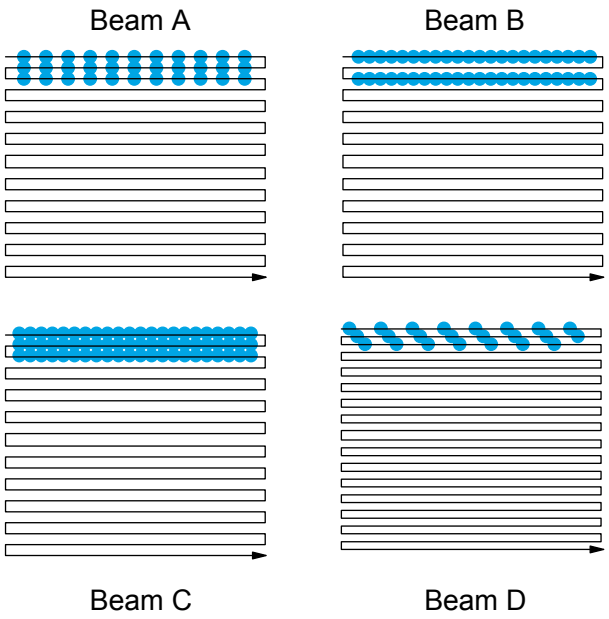

Figure 26 Writing scheme of the patterns in the experiment.

dimension to the scanner field in width. Because there is no mask to scan, the scanning does not have to be reversed for each field as in the case of an optical scanner and the field can be as long as the size of the wafer permits.

Figure 25 shows recent results from a 110-beam head. Four beams were programmed to write distinct patterns such as 80-nm gratings in x, y, 45^0 to the normal, and a completely filled block 2x2 μm^2 in size. The patterns were not proximity corrected. Some resist residue is seen due to insufficient exposure. The significance of this result is that the entire 110-beam e-beam column including the CMOS circuits and the fiber bundle is successfully assembled. The system is working, starting from sending the optical signal to forming controlled patterns in the resist. Figure 26 depicts how the writing is done for the 4 patterns. Currently, electronic defection in both the x and the y direction is used to substitute for mechanical scanning in the y direction. The beams are defected identically just as in a raster scanning system. Different patterns are created by properly blanking the beam with the optical signal. Beam C is run without any blanking. With beam A, the blanking is done at each alternate beam position. Beam B is blanked off at every alternate row. The blanking of beam D is similar to that of beam A except with a phase shift at each consecutive row.

6.4. Challenges in MEB DW systems

E-beam direct write has been in production decades ago[61]. It is being used for product development to date[62]. Still, many challenges lie ahead for high-throughput MEB DW systems. Basically, electron has extremely short wavelength. At a relatively low 5keV energy, the wavelength is 0.0173 nm, approximately 5 orders of magnitude shorter than that of EUV. It is not diffraction limited. The most severe fundamental limit of resolution is caused by scattering in the recording medium, i.e. the resist. The scattering crossection is approximately proportional to the atomic number[63] of the resist and is a function of its depth in the resist. Since the atomic number of polymer materials is already quite small, the only way to reduce the scattering crossection is by reducing the resist thickness. For 22-nm features, one may have to use a resist thickness of 50 nm or less for 5 keV beams. Larger thicknesses may be used for 50~100 keV beams.

Shot noise is also a cause of alarm. To maintain a stable exposure, the number of electrons for each pixel has to be kept sufficiently high. Though the actual number has not be convincingly set, it is generally believed to be a few thousands. As a result, as the pixel size becomes smaller, the resist sensitivity has to decrease. More current has to be used to maintain the throughput. As a result, the thermal loading on the wafer increases. Table 2 shows that to maintain 5000 electrons in each half-pitch pixel, e.g. 32x32nm^2 for 32-nm half pitch, the required resist sensitivity is 78 $\mu C/cm^2$, while for 22-nm half pitch, the sensitivity has to be reduced to 165 $\mu C/cm^2$. To expose 300-mm wafers at a throughput of 15 wph at a 5% pattern density, and assuming 20% non-exposing time, a current density of 0.02 $\mu A/cm^2$ is required. With 5 keV beam, the average heat load is 0.1 mW/cm^2. A much higher instantaneous heat load is calculated according to a 13,000 e-beam array covering 26x10 mm^2 at a scan speed of 27.5 mm/sec. A 10.74 $\mu A/cm^2$ current incident on the 26x10 mm^2 area, produces 53.71 mW/cm^2 during the time that the e-beam array passes through a point in the image plane. The heat load can be as high as 681.82 mW/cm^2 for 30% pattern density with 22-nm half pitch. The case of ArF exposure at 150 wph with a scan speed of 550 mm/sec is also shown in the table. The slot width is now 5 mm instead of 10. The average heat load is slightly lower than that of e-beam exposure. However, the instantaneous heat load is almost three times higher than that with e-beam exposure. Since there is no problem handling this level of heat for ArF exposure, there should not be a problem with 5 keV e-beam exposure either. If the e-beam energy is 50 keV instead, the heat load is 10 times higher. The heat tolerance is not yet known.

Table 2 Heat load on the wafer for e-beam and ArF exposures.

Pattern density (%)	HP (nm)	PR sensitivity ($\mu C/cm^2$)	Total current ($\mu A/cm^2$)	Avg Heat load (mW/cm^2)	Total current ($\mu A/cm^2$)	Slot Heat load (mW/cm^2)
5	32	78	0.02	0.10	10.74	53.71
30	32	78	0.12	0.61	64.45	322.27
5	22	165	0.04	0.22	22.73	113.64
30	22	165	0.26	1.29	136.36	681.82
		mJ/cm^2	ArF exposure			
5	32	30	N/A	0.09	N/A	165.00
30	32	30	N/A	0.54	N/A	990.00

Another challenge with e-beam exposure is the loss of throughput by 2^3 for each node advance reducing the feature size by a factor of $\sqrt{2}$. A factor of 2 is lost due to shot noise requiring the same number of electrons per pixel as just discussed. Another factor of 2 is lost from the increased number of pixels in the same field size. The third factor of 2 is

lost by smaller collection angle from the source with smaller spot size. Therefore, to gain back the throughput loss, one has to resort to using 8 times more current by employing higher brightness sources, using more sources, increasing the collection angle, packing the beams closer, increase of beam coverage area, or a combination of these measures.

7. Cost comparison of future lithography systems

Cost is an important concern for future lithography systems. If the cost of future-node products is higher than that of existing products, a primary incentive to move on is lost. Table 3 compares hypothetic cost of lithography systems for 32-nm minimum half pitch. The estimation includes tool utilization, availability, rework, installation, utility, laser pulse, resist, HMDS, developer, topcoat (if applicable), BARC (if applicable), and 2nd etching (if applicable). The water immersion single pass system for the previous node is shown as a reference. Moving to 32-nm half pitch requires double exposure and double processing and two masks per critical layer. The exposure cost almost doubles and the material cost more than doubles because the 1st etch is not counted across all technologies. EUV lithography was estimated with combinations of high-low cost and high-low throughput. Even at 10 wph for direct write, the number of wafers that breakeven with masked exposure is in the thousands. Five years later, after the exposure tools are fully depreciated, the number of breakeven wafers becomes tens of thousand.

Table 3 Hypothetic cost of 32-nm half pitch lithography technologies.

	H_2O Imm Single Pass	H_2O Imm Double Pass	EUV 40M/100	EUV 40M/20	EUV 50M/100	EUV 50M/20	MEB DW 20M/10
Expo Tool Cost (M Euro)	30	40	40	40	50	50	20
Track Cost (M JPY)	700	700	700	300	700	300	300
Raw Througput (wph)	120	200	100	20	100	20	15
Exposure cost per layer (US$)	16	31	27	126	33	156	88
Mask cost per layer (US$)	80,000	160,000	120,000	120,000	120,000	120,000	N/A
Exposure+material per layer (US$)	24	56	35	134	41	164	93
DW Breakeven Wafers	1,159	4,324	2,069	∞	2,308	∞	Ref
DW Breakeven Wafers after 5 yrs	19,048	∞	38,710	∞	48,000	∞	Ref

8. Conclusion

Through out the history of microlithography, regardless of the means of imaging, proximity or projection, e-beam, ion-beam or photon beam, the mask technology and/or mask cost always stand out as a difficult issue, preventing the imaging technology to progress too far. Mask cost and technology challenges have come to a point that it makes sense to pursue maskless imaging technology. E-beam technology has always been treated as an expensive racehorse. With many new ways such as micro columns using beam-defining apertures, MEMS, or CMOS circuits, to assemble hundreds, ten thousands, even millions of beam or pixel does not seem to be too much of a problem. MEB DW has the potential to be economical and fast. However, we have outlined many challenges on either NGL candidate. Concerted industrial efforts are required to bring them to manufacturing-worthy status with the necessary infrastructure. Of course, the law of economy always has to work within the realm of the law of physics.

The history of microlithography may be making a turn. The most expensive component of an exposure tool has always been the imaging optics. With MEB DW, a large portion of cost is transferred to electronic components which has a much steeper cost-reduction path than optical components. For the first time, the semiconductor industry has an opportunity to self-support cost reduction.

TABLES

FIGURES

Figure 21 KLA-Tencor reflected e-beam lithography (REBL) system.

Figure 22 Transforming an inspection tool to REBL.

Figure 23 Configuration and components of the MAPPER MEB DW system.

Figure 24 The MAPPER writing scheme.

Figure 25 Recent pattern-writing results from optical fiber switching through the imaging assembly to the resist on wafer.

Figure 26 Writing scheme of the patterns in the experiment.

---

[1] D.R. Harriot, “Strategies in lithography”, J. Vac. Sci. Technol. Vol. 12, p. 1121, 1975.
[2] B.J. Lin, “Deep-uv lithography”, J. Vac. Sci. Technol. Vol. 12, p. 1317-1320, 1975.
[3] R. Feder, “Replication of 0.1-μm geometries with x-ray lithography”, J. Vac. Sci. Technol. Vol. 12, pp. 1332-1335 1975.
[4] R. C. Henderson, A.M. Voschenkov, G.E. Mahoney, “Pattern generation on wafers using the electron-beam exposure system (EBES)”, J. Vac. Sci. Technol. Vol. 12, pp. 1261, 1975.
[5] A.J. Speth, A.D. Wilson, A. Kern, T.H.P. Chang, “Electron-beam lithography using vector-scan techniques”, J. Vac. Sci. Technol. Vol. 12, pp. 1235-1239, 1975.
[6] H.C. Pfeiffer, “New imaging and deflection concept for probe-forming microfabrication systems”, J. Vac. Sci. Technol. Vol. 12, pp. 1170-1173, 1975.
[7] J.P. Ballantyne, “Electron-beam fabrication of chromium master masks”, J. Vac. Sci. Technol. Vol. 12, pp. 1257-1260, 1975.
[8] M.B. Heritage, “Electron-projection microfabrication system”, J. Vac. Sci. Technol. Vol. 12, pp. 1135-1140, 1975.
[9] B.J. Lin, "The Future of Subhalf-Micrometer Optical Lithography", Microcircuit Engineering 87, Sept. 1987.
[10] B.J. Lin, "Quarter- and Sub-Quarter Micrometer Optical Lithography", Proceedings of the Symposia on Patterning Science and Technology II, ECS Vol. 92-6, p. 3, 1991.
[11] B.J. Lin, “Optical lithography – present and future challenges”, Comptes Rendus Physique, 7 (2006) 858-874.
[12] B.J. Lin, “The Ending of Optical Lithography and the Prospects of its Successors”, Microelectronic Engineering vol. 83 (2006) pp. 604-613.
[13] Ming-Jiun Yao, Tzu-Yi Wang, Chia-Jen Chen, Hsin-Chang Lee and Yao-Chang Ku, “Application of Sigma7500 pattern generator to X Architecture and 45-nm generation mask making”, to be published.
[14] H.I. Smith, “X-ray lithography: A complementary technique to electron beam lithography”, J. Vac. Sci. Technol. Vol. 10, pp. 913 1973.
[15] H. Bohlen, J. Greschner, W. Kulcke, P. Nehmiz, Proceedings of the 8th International Conference on electron and ion beam science and technology, pp. 406-419, 1978.
[16] T. Utsumi, “Low-energy e-beam proximity projection lithography”, SPIE Proceedings, Vol. 3676, p. 117-125, 1999.
[17] B.J. Lin, "Electromagnetic Near-Field Diffraction of a Medium Slit", J. Opt. Soc. Am., Vol. 62, p. 977-981, 1972.
[18] B.J. Lin, "Optical Methods for Fine Line Lithography", book chapter from "Fine Line Lithography", edited by R. Newman, North-Holland Publishing Co., p. 120, 1980.
[19] B.J. Lin, "A Comparison of Projection and Proximity Printings -- From UV to X-Ray", Microelectronic Engineering vol. 11, p. 137, Elsevier Science Publishers B.V., 1990.
[20] B.J. Lin, "A New Perspective on Proximity Printing -- From UV to X-Ray", J. of Vac. Sci. Technol. B, vol. 8, 1990.
[21] H.K. Oertel, M. Weiss, H.L. Huber, “Modelling of illumination effects on resist profiles in x-ray lithography”, SPIE Proceedings Vol. 1465, p. 244-253, 1991.
[22] J. P. Silverman, “Challenge and progress in x-ray lithography” J. Vac. Sci. Technol. B16, pp. 3137-3141, 1998.
[23] Yuichi Utsumi and Takefumi Kishimoto, “Large area and wide dimension range of x-ray lithography for lithographite, galvanoformung, and abformung process using energy variable synchrotron radiation”, J. Vac. Sci. Technol. Vol. B23, pp. 2903, 2005.
[24] P.J. Heard, J.R.A. Cleaver, H.A. Ahmed, “Application of a focused ion-beam system to defect repair of VLSI masks”, J. Vac. Sci. Technol. Vol. B3, pp 87, 1985.

[25] T. Liang, E. Frendberg, D. Bald, M. Penn, A. Stivers, "E-beam mask repair: Fundamental capability and applications", SPIE Proceedings Vol. 5567, p. 456-466, 2004.
[26] H. Loeschner, H. Buschbeck, M. Ecker, C. Horner, E. Platzgummer, G. Stengl, M. Zeininger, P. Ruchhoeft, J.C. Wolfe, "Masked ion beam lithography and direct-structuring on curved surfaces", SPIE Proceedings Vol. 5037, p. 156-161, 2003.
[27] R.L. Seliger, R.L. Kubena, R.D. Olney, J.W. Ward, V. Wang, "High-resolution ion-beam processes for microstructure fabrication", J. Vac. Sci. Technol. Vol. B16, pp. 1610, 1979.
[28] (Ion beam dissecting and failure analysis)
[29] (1st article for ion beam projection)
[30] (Korean IPL article)
[31] (Loeschner IPL article)
[32] H.S. Hemstreet, D.A. Markle, W.H. Newell, A. Offner, "Optical Projection Apparatus", US Patent 4,011,011, 1977.
[33] D.A. Markle "A new projection printer", Solid State Technology, June 1974, p. 50.
[34] R. Hershel, "Optics in the Model 900 projection stepper", SPIE Proceedings, Vol. 221, p. 39, 1980.
[35] D. Markle, "The future and potential of optical scanning systems", Solid State Technology, Vol. 27, p. 159, Sept. 1984.
[36] T. Fahey, J. McClay, M. Hansen, B. tirri, M. Lipson, "SVG 157nm Lithograephy technical review", SPIE Proceedings vol. 4346, p. 72-80, 2001.
[37] ASML 1400 scanner.
[38] ASML 1900i scanner
[39] W. Ulrich, H.J. Rostalski, R. Hudyma, "Development of dioptric projection lenses for deep ultraviolet lithography at Carl Zeiss", J. Microlith., Microfab., Microsyst., vol. 3, p. 87-96, 2004.
[40] B.J. Lin, "Semiconductor Foundry, Lithography, and Partners", SPIE Proceedings Vol. 4688, p. 11, 2002.
[41] B.J. Lin, "Lithography for manufacturing of sub-65nm nodes and beyond", IEDM 05-53, pp. 3.1.1-3.1.4, 2005.
[42] Jeng-Horng Chen, Li-Jui Chen, Tun-Yung Fang, Tzung-Chi Fu, Lin-Hung Shiu, Yao-Te Huang, Norman Chen, Da-Chun Oweyang, Ming-Che Wu, Shih-Che Wang, John C.H. Lin, Chun-Kuang Chen, Wei-Ming Chen, Tsai-Sheng Gau, Burn J. Lin, Richard Moerman, Wendy Gehoel-van Ansem, Eddy van der Heijden, Fred de Johng, Dorrothe, Oorschot, Herman Boom, Martin Hoogendorp, Chrristian Wagner, Bert Koek, "Characterization of ArF immersion process for production", SPIE Proceedings, Vol. 5754, pp. 13-22, 2005.
[43] B.J. Lin, "Depth of Focus in Multi-Layered Media – A Long-Neglected Phenomenon Aroused by Immersion Lithography", J. Microlith., Microfab., Microsyst., Vol. 3, p 21-27, 2004.
[44] B.J. Lin, "Simulation of optical projection with polarization-dependent stray light to explore the difference between dry and immersion lithography", J. Microlith., Microfab., Microsyst., Vol. 3, p 9-20, 2004.
[45] T.S. Gau, C.K. Chen, B.J. Lin, "The Image Characterization of Bubbles in water for 193-nm Immersion Lithography", J. Microlith., Microfab., Microsyst., Vol. 3, p 61-67, 2004.
[46] B.J. Lin, "Immersion lithography and its impact on semiconductor manufacturing", J. Microlith., Microfab., Microsyst., Vol. 3, p. 377-395, 2004.
[47] C.Y. Chang, D.C. Yu, J.H. Chen, C.H. Lin, B.J. Lin, J.W. Thackeray, V. Vohra, G. Wayton, T. Kurihara, "A Novel Switchable BARC (SBARC) and Process to Improve Pattern Collapse and Defect Control", SPIE Proceedings, Vol. 6153, p. 61530M1-10, 2006.
[48] C.Y. Chang, D.C. Yu, C.H. Lin, B.J. Lin, "Watermark Defect Formation and Removal for Immersion Lithography", SPIE Proceedings, Vol. 6154, p. 6154171-8, 2006.
[49] C.Y. Chang, D.C. Yu, C.H. Lin, B.J. Lin, "Development of Cleaning Process for Immersion Lithography", SPIE Proceedings, Vol. 6154, p. 61544R1-11, 2006.
[50] F.J. Liang, H.Chang, L.H. Shiu, C.K. Chen, L.J. Chen, T.S. Gau, and B.J. Lin, "Immersion Defect Reduction (1) - Analysis of Water Leaks in an Immersion Scanner, SPIE Proceedings Vol. 6520-193, 2007.
[51] Lin-Hung Shiu, Fu-Jye Liang, Hsing Chang, Chun-Kuang Chen, Li-Jui Chen, Tsai-Sheng Gau, and Burn J. Lin, "Immersion Defect Reduction (2) -- The Formation Mechanism and Reduction of Patterned Defects, SPIE Proceedings Vol. 6520-38, 2007.
[52] H. Kinoshita, K. Kurihara, Y. Ishii, Y. Torii, "Soft x-ray reduction lithography using multilayer mirrors," J. Vac. Sci. Technol. Vol B7, p. 1648, 1989.
[53] J.E. Bjorkholm, J. Bokor, L. Eichner, R.R. Freeman, T.E. Jewell, W.M. Mansfield, A.A. Macdowell, E.L. Raab, W.T. Silfvast, L.H. Szeto, D.M. Tennant, W.K. Waskiewicz, D.L. White, D.L. Windt, O.R. Wood II, and J.H. Brunning,

"Reduction imaging at 14 nm using multilayer-coated optics: Printing of features smaller than 0.1 μm," J. Vac. Sci. Technol., Vol. B8, p. 1509, 1990.
[54] B.J. Lin, "Sober view on EUV lithography", J. Microlith., Microfab., Microsyst., Vol. 5, pp. 1537, 2006.
[55] H. Meiling, V. Banine, P. Kurz, N. Harned, "Progress in the ASML EUV program," SPIE Proceedings, Vol. 5374, p. 31-42, 2004.
[56] H. Meiling, V. Banine, N. Harned, B. Blum, P. Kurz, H. Meijer, "Development of the ASML EUV alpha demo tool," SPIE Proceedings, Vol. 5751, p. 90-101, 2005.
[57] Takaharu Miura et al, "Nikon EPL tool: The latest development status and results", SPIE Proceedings vol. 5751, p. 477-482, 2005.
[58] Courtesy MultiBeam Systems.
[59] Courtesy KLA-Tencor.
[60] Courtesy MAPPER Lithography b.c.
[61] H.C. Pfeiffer, "Direct write electron beam lithography – A production line reality", Solid State Technology, vol. 27, p. 223, 1984.
[62] L. Pain et al, "Electron beam direct write lithography flexibility for ASIC manufacturing a opportunity for cost reduction", SPIE Proceedings, Vol. 5751, p. 35-45, 2005.
[63] T.E. Everhart, "Simple theory concerning the reflection of electrons from solids", J. Appl. Phys. Vol. 31, p. 1483-1490, 1960.